CORROSION SCIENCE AND TECHNOLOGY, Vol.31, No.5(2002), pp.361~367

Effect of Heat Treatment on the Pitting Corrosion Behavior of 347 SS Weld Overlay

I. H. Lo, M. C. Lee*, K. Y. Lin*, W. Ho*, G. C. Y. Yang*, and W. T. Tsai

Department of Materials Science and Engineering
National Cheng Kung University
Tainan, Taiwan
**Formosa Petrochemical Corporation*
Yunlin, Taiwan

The effect of heat treatment on the microstructural change and corrosion performance of 347 SS weld overlay has been investigated. The microstructure and phase changes of he as-weld and post weld heat-treated (PWHT) overlays were examined using optical microscropy (OM), scanning electron microscopy (SEM) and transmission electron microscopy (TEM). Energy dispersive X-ray analysis (EDS) was also used for intermetallic phase identification. The results showed that delta-ferrite transformation to sigma phase occurred for the as-weld overlay by PWHT at 690℃ for 8 hours. Pitting corrosion resistance of the weld with or without PWHT was evaluated by conducting potentiodynamic polarization tests in 3.5 % NaCl solution. The results showed that the presence of intermetallic phase greatly affected the pitting corrosion resistance of 347 SS weld overlay.

Keywords *: 347SS overlay weld, post weld heat treatment (PWHT), sigma phase, pitting corrosion*

1. Introduction

Overlay welding of Type 347 stainless steel (SS) is incorporated in the manufacture of petroleum hydrodesulfurization reactor made of 2.25Cr-1Mo pressure vessel steel. Two types of cladding, namely single-layer overlay welding of Type 347 SS and double-layer overlay welding of Type 347 SS over Type 309 SS, respectively, are commonly used. In both cases, post weld heat treatment (PWHT) at 690℃ for several hours is always applied after the overlay welding or the attachment of the internal structures.[1-2)]

In the weld of austenitic SSs, at least 5%, by volume, of δ-ferrite in the microstructure is required to minimize the thermal cracking during the weld solidification.[3),4)] On the other hand, Thommas has noted that the ductility of the weld is reduced when the δ-ferrite content is higher than 10%.[4)] For austenitic SS weld, the relaxation of thermal residual stress and the improvement of ductility can be achieved by PWHT.[1)] However, phase transformation or precipitation of carbides may occur in the metastable austenite/ferrite weld during PWHT. One intermetallic phase known as σ-phase can be transformed fromδ -ferrite when heat treated at elevated temperature.[1),5),6)]

The disbonding[7)] and cracking[8),9)] of Type 347 SS weld overlay have always been of great concern. Recently, however, pitting corrosion of Type 347 weld overlay has also been reported.[10)] The formation of intermetallic compounds during PWHT might affect the pitting corrosion behavior. Thus, the types of intermetallic compounds formed in Type 347 SS overlay weld after PWHT, and their effects on the pitting susceptibility are of interested and investigated in this study.

2. Experimental

Submerged arc welding (SAW) was employed to prepare the overlay weld of Type 347 SS over Type 309L SS plate. Two different electrodes were used and the respective chemical compositions of the welds are listed in Table 1. For sample SL in Table 1, no heat treatment was applied after welding. While for sample ML, post weld heat treatment (PWHT) at 690 ℃ for 8 h was carried out.

Microstructure analysis and phase identification were performed by conducting transmission electron microscopy (TEM) using a Hitachi 2000 field emission transmission

Table 1. Chemical compositions of major alloying elements in Type 347 SS overlay welds

Element wt% / Sample	C	Si	Mn	Cr	Ni	Nb	Mo	Cu	Fe
SL	0.047	0.606	1.30	17.21	9.74	0.532	0.186	0.064	Bal.
ML*	0.030	0.450	2.10	19.00	9.50	0.500	0.060	0.070	Bal.

*PWHT at 690℃/8h

Table 2. TEM/EDS chemical composition analysis for major alloying elements. (Wt. %)

Sample	Element / Phase	Fe	Cr	Ni	Nb	O	Remarks
SL	γ	68.67	21.71	9.62	–	–	F in Fig. 1(a)
	δ	67.27	27.64	5.08	–	–	G in Fig. 1(a)
	NbC	39.89	11.37	3.84	44.93	–	H in Fig. 1(a)
	Oxide	30.13	17.51	4.69	1.32	Bal.	I in Fig. 1(a)
ML	γ	69.25	19.75	11.00	–	–	A in Fig. 3(a)
	δ	62.20	28.72	7.08	2.00	–	B in Fig. 3(a)
	$Cr_{23}C_6$	60.17	27.56	3.09	9.17	–	C in Fig. 3(a)
	NbC	1.78	1.00	–	97.22	–	D in Fig. 3(a)
	σ	65.99	34.10	–	–	–	E in Fig. 3(a)

electron microscope operating at 200kV. This microscope was equipped with an energy-dispersive X-ray spectrometer (EDS) for chemical analysis.

The susceptibilities of the as-welded and the PWHT Type 347 SSs to pitting corrosion in 3.5 wt% NaCl solution were evaluated by conducting open circuit potential (OCP) and potentiodynamic polarization curve measurements.

3. Results and discussion

3.1 Microstructure and phase analyses

Fig. 1(a) is a bright field electron micrograph of the as-welded 347 SS overlay (sample SL). Clearly, it consists of a primary phase (marked as "F"), a secondary phase (marked as "G"), and some other precipitates (marked as "H" and "I"). Fig. 1(b) is a selected-area diffraction (SAD) pattern detected from phase "F". Only face-centered cubic (fcc) diffraction spots are observed, indicating that the primary phase (marked as "F" in Fig. 1) is austenite phase (γ). Fig. 1(c) shows another SAD pattern taken from the secondary phase marked as "G" in Fig. 1(a). The result shows only body-centered cubic (bcc) diffraction spots of δ ferrite phase appeared in the SAD pattern. The contents of the major alloying elements analyzed by using EDS

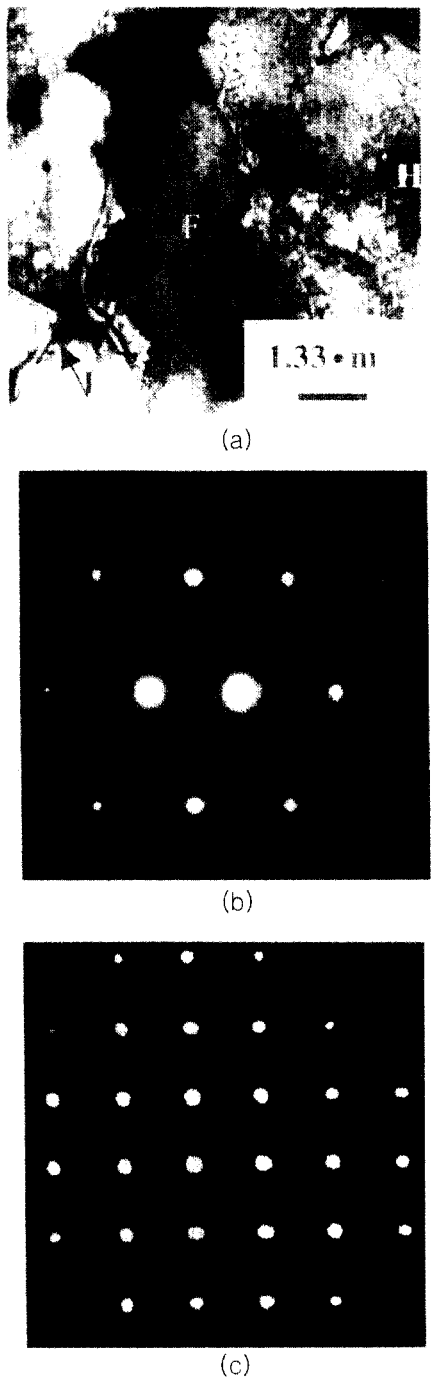

Fig. 1. (a) Bright field image of welding overlap without PWHT. (b) SADP taken from grain "F" and its foil normal is [011] for austenite phase. (c) SADP taken from grain "I" and the foil normal is [011] ferrite phase

for the spots F and G in Fig. 1 are shown in Table 2. The results reveal that spot F has a higher Ni and a lower Cr contents, while the relative Ni and Cr contents are reversed for the spot G. The EDS results are consistent with TEM analysis.

Fig. 2(a) shows the bright field electron micrograph of precipitate "I" located on the γ / δ boundary. According to the SAD pattern shown in Fig. 7(b) and the EDS results depicted in Table 2, the fcc type diffraction spots are corresponding to niobium carbide.[11] The dark field electron micrograph shown in Fig. 2(c) confirms that the precipitate marked as "I" in Fig. 1(a) is NbC. The spot marked as "H" in Fig. 1(a) is an oxide as identified by EDS. After detail TEM examination, no other precipitates beside NbC are found in sample SL (as-welded).

The bright field electron micrograph of the PWHT Type 347 SS weld is shown in Fig. 3. The SAD pattern consists of two different crystal structures as demonstrated in Fig. 4(a) and (b). The foil normal of Fig. 4(a) is [011], and the diffraction spots belong to austenite phase.[12] In Fig. 4(b), the foil normal is [011] and the diffraction spots are for δ ferrite phase.[12] Fig. 4(c) is the dark field image of austenite phase, taken from spot "A" under the condition of the zone axis near exact [011]. The dark field image of ferrite phase, taken from grain "B" under the condition of the zone axis near exact [011] is demonstrated in Fig. 4(d).

Similar to that found in the as-welded Type 347 SS overlay, NbC is found inside the austenite phase. The bright field and dark field images as well as the SAD pattern of the rod-like NbC precipitate (marked as "D" in Fig. 3) are shown in Fig. 5.

Fig. 6(a) is a bright field image of the precipitate marked as "C" inside grain "A"(austenite phase) in Fig. 3. Fig. 6(b) shows the SAD pattern taken from the precipitate and its surrounding austenite matrix. From the camera length and d-spacings of the diffraction spots, the crystal structure of the precipitate was determined to be $Cr_{23}C_6$ having a face-centered cubic structure. Fig. 6(c) is the dark field image of $Cr_{23}C_6$.

Most importantly, a bar-like precipitate is found on the γ / δ grain boundary (marked as "E" in Fig. 3) as illustrated by the bright field image in Fig. 7(a). Fig. 7(b) shows the SAD pattern obtained from the bar-like

(a)

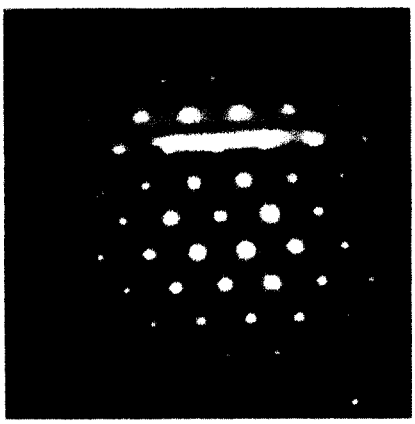

(b)

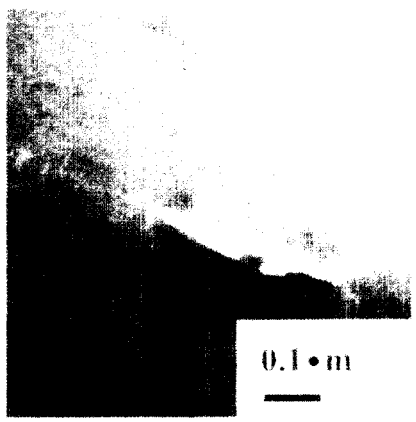

(c)

Fig. 2. (a) Bright field electron micrograph of NbC, marked as "I" in Fig. 6 (a). (b) SADP taken from NbC and its foil normal is [001]. (c) Dark field electron micrograph of NbC.

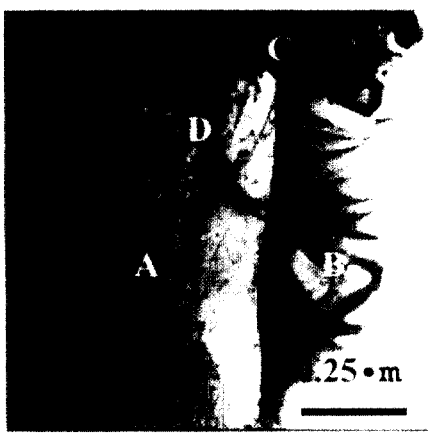

Fig. 3. Electron micrograph of overlay weld with post-weld heat treatment (690℃/8h).

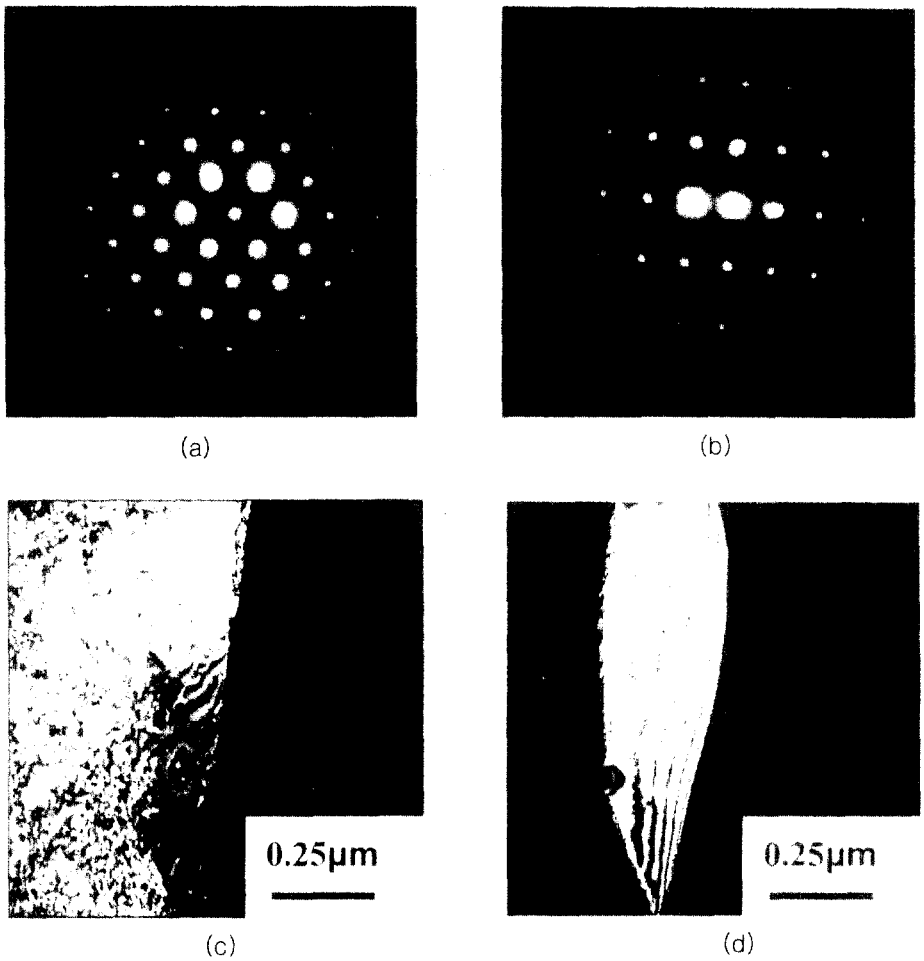

Fig. 4. (a) SADP taken from grain "A" and its foil normal is [011] for austenite phase. (b) SADP taken from grain "B" and the foil normal is [011] ferrite phase. (c) Dark field electron micrograph of grain "A". (d) Dark field electron micrograph of grain "B".

Fig. 5. (a) Bright field electron micrograph of NbC, marked as "D" in Fig. 1. (b) SADP taken from NbC and its foil normal is [011]. (c) Dark field electron micrograph of NbC.

precipitate. From the SAD pattern and the EDS result shown in Table 2, this precipitate with a body-centered tetragonal (bct) structure is identified as sigma (σ) phase. The dark field electron micrograph of σ phase precipitated in the PWHT Type 347 SS overlay is shown in Fig. 7(c). The formation of σ phase resulting from the eutectoid

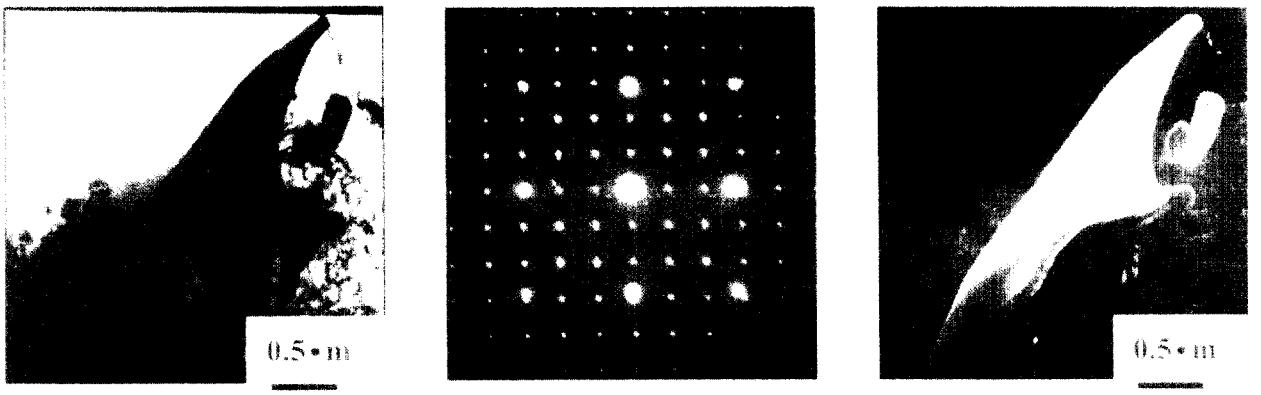

Fig. 6. (a) Bright field electron micrograph of $Cr_{23}C_6$, marked as "C" in Fig. 1. (b) [001] SADP taken from $Cr_{23}C_6$ and its surrounding austenite matrix. (c) Dark field electron micrograph of $Cr_{23}C_6$.

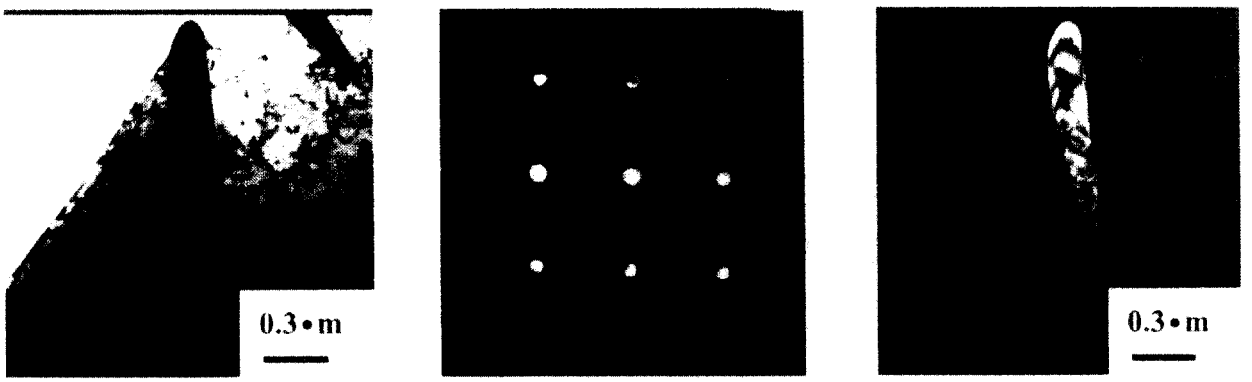

Fig. 7. (a) Bright field electron micrograph of σ, marked as "E" in Fig. 1. (b) SADP taken from σ-phase and its foil normal is [001]. (c) Dark field electron micrograph of σ-phase.

decomposition of δ ferrite phase, $\delta \rightarrow \gamma' + \sigma$, in the temperature range 600~690℃ has been extensively reported in the literature.[1),3),5),13),14)]

3.2 Corrosion evaluation

The open circuit potentials (OCP) of Type 347SS overlays, as-welded and PWHT, determined in deaerated 3.5 wt% NaCl solution are measured. The OCP of the as-welded Type 347 SS is about -420 mV, with respect to a saturated calomel electrode (SCE). For the PWHT overlay weld, the OCP is about -290 mV(SCE), which is about 130 mV higher than that of the as-welded overlay. PWHT certainly affects the electrochemical property of the 347 SS overlay weld.

The potentiodynamic polarization curves of Type 347 SS overlays, with or without PWHT, in deaerated 3.5 wt% NaCl solution are shown in Fig. 8. The results show that pitting initiation potential of the as-welded Type 347 SS overlay is about 200 mV higher than that of the PWHT, indicating that the as-welded overlay is more resistant to

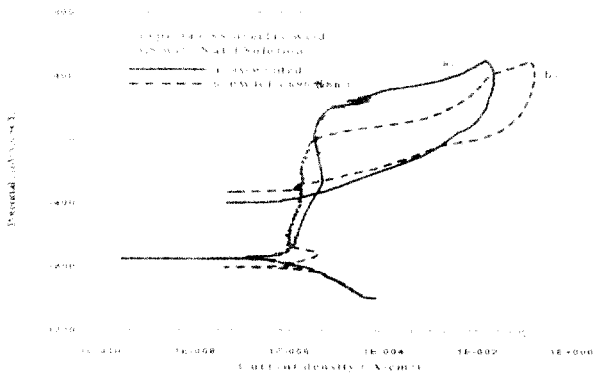

Fig. 8. Potentiodynamic polarization curves for Type 347 SS overlay welds, as-welded and with PWHT, in deaerated 3.5 wt% NaCl solution.

pit initiation in 3.5 wt% NaCl solution. As can be seen in Fig. 8, the pitting corrosion protection potential of 347 SS overlay with PWHT is about -300 mV(SCE), while that of the as-welded overlay is about -350 mV(SCE). Since the OCP (-420 mV) of the as-welded overlay in

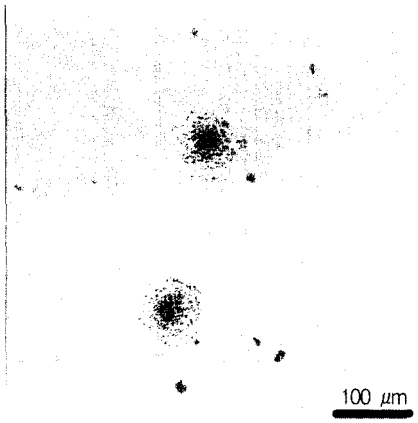

(a)

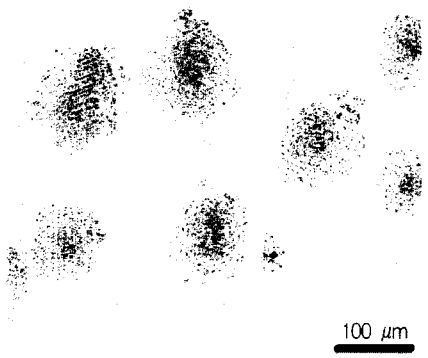

(b)

Fig. 9. Pits formed on the surfaces of Type 347 SS overlay welds after potentiodynamic polarization curve measurements in deaerated 3.5 wt% NaCl solution, (a) as-welded, and (b)PWHT.

deaerated 3.5 wt% NaCl solution is lower than its pitting protection potential (-350 mV), pitting corrosion will be difficult to proceed even defects may exist on the surface. However, for the PWHT overlay, since the OCP (-290 mV) is higher than its pitting protection potential (-300 mV), pitting propagation may occur if defects appear on the surface of the overlay. The potentiodynamic polarization curves demonstrate that the overlay with PWHT has a higher susceptibility to pitting corrosion as compared with the as-welded. Fig. 9 shows that the density of pits on the as-welded overlay (Fig. 9(a)) is lower than that on the PWHT (Fig. 9(b)) after potentiodynamic polarization curve measurements. The most susceptible site of Type 347 SS overlay is found to locate at the δ /γ interface as revealed in the SEM micrograph (Fig. 10). The presence of σ phase, preferentially formed in the δ / γ interface, is the main cause for the increase of pitting corrosion susceptibility.

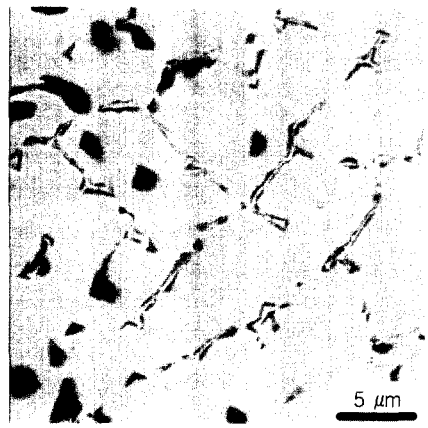

Fig. 10. Pit formed in the δ /γ interface for the PWHT Type 347 SS overlay weld, after potentiodynamic polarization curve measurement in deaerated 3.5 wt% NaCl solution.

The adverse effects of sigma phase and carbides on the corrosion performance of welds have long been recognized.[1),15),16)] Wang et al[17)] have also indicated that continuous network ofδ ferrite is deleterious to pitting corrosion and cracking resistance. The local composition change resulting from phase transformation or precipitation and the difference in the electrochemical activity between any two adjacent phases are the main factors controlling the corrosion performance of the welds.

4. Conclusions

1) In the as-welded Type 347 SS overlay, δ ferrite and NbC are found in the austenitic matrix. Post weld heat treatment at 690°C for 8 hours results in the formation of $Cr_{23}C_6$ and σ phase in the overlay weld.

2) The presence of σ phase resulting from eutectoid decomposition of δ ferrite causes an increase in the pitting corrosion susceptibility of Type 347 SS overlay weld.

References

1. J. J. Smith and R. A. Farrar, *International Materials Reviews*, **38**, 25 (1993).
2. R. Kayano, K. Kimura, H. Tokushige, and T. Ishiguro, in Proc. Of "The 1998 ASME/JSME Joint Pressure Vessels and Piping Conference, Fitnee-for-service Evaluations in Petroleum and Fossil Power Plants", July 26-30, 1998, San Diego, CA, USA, PVP-Vol. 380, ASME, 317-324 (1998) .
3. Y. Song, T. N. Baker, N. A. McPherson, *Materials Science and Engineering*, **A212**, 228 (1996).
4. R. G. Thomas, *Weld. J.*, **57**, 81s(1978).
5. M. Schwind, J. Kallqvist, J. -O. Nilsson, J. Agren, and H. -O. Andren, *Acta Mater.* **48**, 2473 (2000).
6. Karlsson, *et al.*, Applications of stainless steel '92,

Stockholm, Jarn Kontoret, 335-344 (1992).
7. M. De Sanctis, L. Paganini, A. Solina, and R. Valentini, *J. Heat Treat.*, **7**, 35 (1989).
8. R. W. Messler Jr., and L. Li, *Science and Technology of Welding and Joining*, **2**, 43 (1997).
9. E. W. Johnson, Welding Research Council, Bulletin, Aug., 240 (1978).
10. Internal Report, Formosa Petrochemical Company.
11. R. M. Tsong, M. Schmid, C, Nagl, P. Varga, R. F. Davis, and I. S. T. Tsong, *Surface Science* **366**, 85 (1996).
12. David B. Williams and C. Barry Cater, in Transmission Electron Microscopy Ch.18 281~282 (1995).
13. T. P. S. Gill, V. Shankar, M. G. Pujar, and P. Rodriguez, Scripta Metall., **32**, 1595 (1995).
14. S. S. Babu, S. A. David, J. M. Vitek, and M. K. Miller, *Applied Surface Science*, **87/88**, 207 (1995).
15. A. J. Sedriks, *Int. Metals Reviews*, **28**, 295 (1983).
16. T. P. S. Gill, J. B. Gananamoorthy, and K. A. Padmanbhan, *Corrosion*, **43**, 208 (1987).
17. Wang Zheng, Xu Xiang-Jun, and Ren Chen-Xing, in Proc. of The Cross-Strait Conference on Materials Corrosion and Prevention, Chang-Jian Lin and Wen-Ta Tsai (Eds.), Xiamen, China, October 25-28, 201 (1998).